Biochemical and Biophysical Research Communications 431 (2013) 398–403

Contents lists available at SciVerse ScienceDirect

Biochemical and Biophysical Research Communications

journal homepage: www.elsevier.com/locate/ybbrc

ALS-causing P56S mutation and splicing variation on the hVAPB MSP domain transform its β-sandwich fold into lipid-interacting helical conformations

Haina Qin [a], Wei Wang [a], Jianxing Song [a,b,*]

[a] Department of Biological Sciences, Faculty of Science, Yong Loo Lin School of Medicine and National University of Singapore, 10 Kent Ridge Crescent, Singapore 119260, Singapore
[b] Department of Biochemistry, Yong Loo Lin School of Medicine and National University of Singapore, 10 Kent Ridge Crescent, Singapore 119260, Singapore

ARTICLE INFO

Article history:
Received 3 January 2013
Available online 16 January 2013

Keywords:
Amyotrophic lateral sclerosis (ALS)
VAPB
Protein aggregation
Chameleon transformation
Dodecylphosphocholine (DPC)
NMR spectroscopy

ABSTRACT

P56S mutation on VAPB MSP domain causes a familial ALS, characteristic of severe aggregation both *in vivo* and *in vitro*. We previously showed that P56S rendered the MSP domain to be predominantly disordered in water. Unexpectedly, here we reveal that P56S-MSP transforms into a highly helical conformation in a membrane environment. This chameleon transformation is shared by a splicing variant VAPB-3 with a truncated MSP domain, which is also highly disordered and buffer insoluble as demonstrated here by NMR. Our discovery provides a mechanism for ALS-causing VAPB mutants/variants to gain novel functions such as to mediate ER structure before significant accumulation of aggregates occurs.

1. Introduction

Amyotrophic lateral sclerosis (ALS) is a rapidly progressive and the most prevalent fatal motor neuron disease with death occurring within 1–5 years of the disease onset, characteristic of loss of both upper and lower motor neurons. ALS affects people of all race and ethnic background and approximately 10% of the cases have hereditary background while the rest are sporadic. Since sporadic and familial ALS bear a remarkable similarity in clinical manifestations, it is thought that knowledge and therapeutic approaches/agents developed on mutant models can be translated to sporadic ALS. So far, no effective therapy exists to slow down the course of the disease [1,2].

To date, about 10–13 ALS-causative genes have been identified and the most characterized ALS1 encodes more than 140 mutants of Cu/Zn–superoxide dismutase (SOD1) [1–3]. ALS8 was identified from a large Brazilian family of Portuguese origin with autosomal dominant motor neuron diseases, which encodes a mutated P56S VAPB (vesicle-associated membrane protein-associated protein B) [4]. The human VAP family proteins include VAPA, VAPB, and several alternatively spliced VAPB variants [5,6]. Despite having very diverse functions, VAPA and VAPB share ~60% sequence identity and are composed of three conserved domains, namely an N-terminal 125-residue domain homologous to the major sperm protein (MSP), a central coiled-coil domain, and a C-terminal transmembrane fragment.

VAP proteins are ubiquitously expressed, type II integral membrane proteins that localize to the endoplasmic reticulum (ER) and pre-Golgi intermediates [7], which have been shown to target lipid–binding proteins carrying a short motif containing two phenylalanines in an acidic tract (FFAT motif) to the ER [8]. Remarkably, the MSP domain has been identified to be cleaved from its transmembrane anchor to serve as a ligand for Eph receptors [9,10], which constitute the largest family of receptor tyrosine kinases and their interactions with ephrin ligands initiate bidirectional signals controlling many physiological and pathological processes [10–12], as well as for Robo and Lar-like receptors acting to modulate mitochondrial localization and morphology [13]. Very recently we found that the NS5A protein of hepatitis C Virus (HCV) also targets the MSP domain, thus implying a linkage of HCV infection to ALS development [14].

Two ALS-causing mutations P56S and T46I [15] are both located in the MSP domain. Recently, several VAPB splicing variants containing truncated MSP domains were also implicated in ALS pathogenesis [6]. For example, VAPB-3 is only composed of N-terminal 105 residues identical to the MSP domain, plus a short unique C-tail. Previously the P56S mutant has been extensively characterized to form very tight aggregates *in vivo*, which were even resistant to solubilization by Triton X-100 [16]. The aggregated inclusions have been proposed to trigger unfolded protein response (UPR) in ER [17], thus leading to ALS pathogenesis. Indeed, we demonstrated

* Corresponding author at: Department of Biological Sciences, Faculty of Science, Yong Loo Lin School of Medicine and National University of Singapore, 10 Kent Ridge Crescent, Singapore 119260, Singapore. Fax: +65 6779 2486.
E-mail address: bchsj@nus.edu.sg (J. Song).

0006-291X/$ - see front matter © 2013 Elsevier Inc. All rights reserved.
http://dx.doi.org/10.1016/j.bbrc.2013.01.039

that the wild-type human MSP domain adopts the typical MSP fold constituted by seven-stranded immunoglobulin-like β-sandwiches with s-type topology. By contrast, the P56S mutation eliminated the native MSP structure and rendered the mutant to be predominantly-disordered as well as highly insoluble in buffer [18]. However, a recent study failed to detect significant formation of inclusions in motor neurons derived from induced pluripotent stem cells of patients carrying the P56S mutation [19]. A just-published study showed that fundamentally different from other aggregated proteins linked to neurodegenerative diseases, the P56S mutant had a unique ability to remodel stacked cisternae of endoplasmic reticulum [20].

Here we report for the first time that unexpectedly the P56S, but not wild-type MSP domain, is able to specifically interact with dodecylphosphocholine (DPC), and subsequently transforms into a helical conformation. Strikingly, this lipid-induced transformation is also shared by VAPB-3. Our results thus provide a mechanism by which the ALS-causing mutants/variants of VAPB initiate ALS development by specifically interacting with membranes even before severe accumulation of aggregated inclusions occurs in the cytosol.

2. Materials and methods

2.1. Cloning, expression, and purification of MSP, P56S-MSP and VAPB-3

The expression and purification of the wild-type MSP domain followed the exact procedure we previously reported [18]. To minimize the effect of the large His-tag (16 residues) in our previous study [18], in the present study DNA fragments encoding P56S-MSP and VAPB-3 were amplified from pET32a constructs by using designed primers, which were subsequently cloned into pET28a vector (Novagen) only with 6 His residues at the C-terminus. The vectors were transformed into *E. coli* BL21 (DE3) cells (Novagen) for protein expression. Both P56S-MSP and VAPB-3 were only found in inclusion body and consequently the pellets were first dissolved in the buffer containing 8 M urea and subsequently purified by the Ni^{2+}-affinity column under the denaturing condition in the presence of 8 M urea. The eluted fractions were further purified by reverse-phase HPLC on a C8 column and lyophilized. The generation of the isotope-labeled proteins for NMR studies followed a similar procedure except that the bacteria were grown in M9 medium with the addition of $(^{15}NH_4)_2SO_4$ for ^{15}N labeling and $(^{15}NH_4)_2SO_4/[^{13}C]$–glucose for ^{15}N–/^{13}C double labeling [18]. The purity of the recombinant proteins were checked by the SDS–PAGE gel and their molecular weights were verified by a Voyager STR matrix-assisted laser desorption ionization time-of-flight-mass spectrometer (Applied Biosystems). The concentration of protein samples was determined by the spectroscopic method in the presence of denaturant [21].

2.2. Determination of solution conformations by CD spectroscopy

All circular dichroism experiments were carried out on a Jasco J-810 spectropolarimeter (Jasco Corporation, Tokyo, Japan) as previously described [10,18]. The CD samples were prepared by dissolving the lyophilized protein powders in Mill-Q water with a concentration of 20 μM at pH 4.0. Far-UV CD spectra were collected at 25 °C for MSP, P56S-MSP and VAPB-3 in the absence and in the presence of DPC at various molar ratios: 1:6; 1:7, 1:8, 1:9, 1:10, 1:20, 1:30, 1:40, 1:50, 1:60, 1:70, 1:80, 1:90, 1:100, 1:110, 1:120, 1:150 and 1:200 (protein:DPC). The estimation of secondary structure contents from CD spectra were conducted by using CDSSTR software [22].

2.3. NMR experiments

All NMR data were collected at 25 °C on an 800 MHz Bruker Avance spectrometer equipped with a shielded cryoprobe as described before [10,18]. For HSQC titrations of MSP, P56S-MSP and VAPB-3 by DPC at molar ratios of 1:2, 1:4, 1:6, 1:8, 1:10, 1:20, 1:30, 1:40, 1:50, 1:60, 1:70, 1:80, 1:100, 1:120, 1:150, 1:200 (protein:DPC), series of two dimensional ^1H–^{15}N HSQC spectra were acquired on ^{15}N-labeled protein samples at a concentration of 100 μM in water at pH 4.0, with gradual addition of DPC.

For achieving sequential assignments, triple-resonance experiments including HNCACB and CBCA(CO)NH were acquired on a ^{15}N–/^{13}C-double-labeled sample of VAPB-3 at a protein concentration of 500 μM in water at pH 4.0. For NOE analysis, ^{15}N-edited HSQC–TOCSY and HSQC–NOESY spectra were acquired for a ^{15}N-labeled VAPB-3 sample at the same protein concentration and pH [10,18].

3. Results

3.1. Conformational transformations as monitored by CD spectroscopy

Previously by CD and NMR spectroscopy we have shown that the P56S-MSP domain with an N-terminal 16-residue His-tag is highly-disordered in water, only with helical conformations weakly-populated over some segments. Here to minimize the effect of the large His-tag, we recloned the P56S-MSP into the vector with only C-terminal 6 His residues for affinity purification. Again, the new P56S-MSP sample still has a far-UV CD spectrum typical of a highly-unstructured protein, with only one negative signal at ~200 nm (Fig. 1A). Very unexpectedly, however, upon gradual

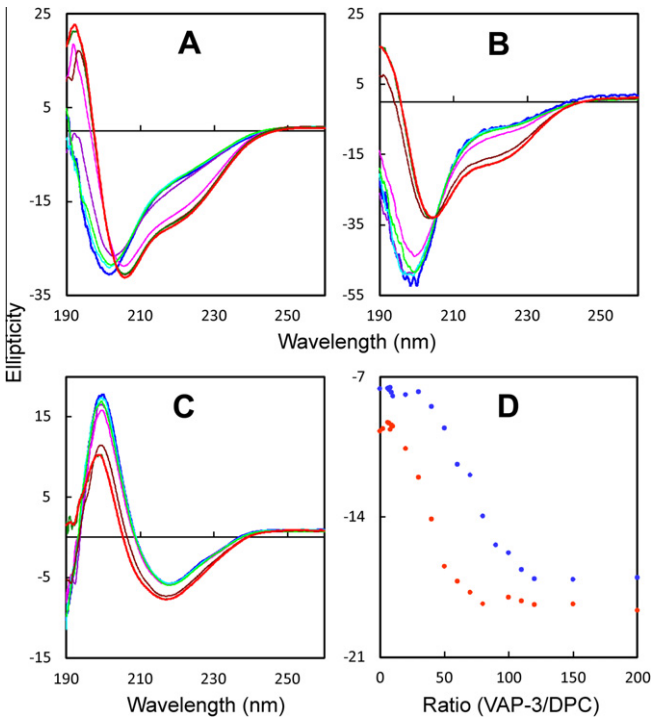

Fig. 1. Conformational transformations as monitored by CD. Far-UV CD spectra of P56S-MSP (A); VAPB-3 (B) and wild-type MSP (C) in the absence of (blue) and in the presence of DPC at different ratios (protein:DPC): 1:6 (cyan), 1:10 (bright green), 1:20 (purple), 1:50 (pink), 1:100 (brown), 1:150 (green) and 1:200 (red). (D) Ellipticity values at 222 nm of P56S-MSP (red) and VAPB-3 (blue) vs. the ratios (protein:DPC). (For interpretation of the references to colour in this figure legend, the reader is referred to the web version of this article.)

addition of DPC, the P56S-MSP started to transform into helical conformations at a ratio of 1:10 and the transformation largely completed at 1:80 (P56S:DPC) (Fig. 1A and D). The far-UV CD spectra at ratios of 1:150 and 1: 200 are almost superimpossible, which have two negative signals, one at ~206 nm and another at ~222 nm, characteristic of helical conformations. Further analysis of the far-UV CD spectrum at 1:150 by CDSSTR software yields to 67.2% helix, 13.1% extended conformation, 8.2% turn and 11.5% random coil contents.

To test whether this transformation is also shared by other VAPB variants, we selected VAPB-3 as it has the N-terminal 105 residues completely identical to the MSP domain and has been proposed to be also involved in ALS pathogenesis [6]. The recombinant VAPB-3 protein was also insoluble in buffer but again could be dissolved in unsalted water as we previously found for a large variety of insoluble proteins [23], as well as the P56S-MSP [18], which was further demonstrated by other groups [24]. Interestingly, VAPB-3 is also highly unstructured as judged from its far-UV CD spectrum in water (Fig. 1B). Strikingly it also underwent the same transformation into a helical conformation upon adding DPC (Fig. 1B). It is worthwhile to point out that the transformation for VAPB-3 started at a ratio of 1:30 and largely completed at 1:100 (VAPB-3:DPC) (Fig. 1B and D). Similar analysis of the far-UV CD spectrum at 1:150 yields to 68.2% helix, 12.1% extended conformation, 7.9% turn and 11.8% random coil contents.

On the other hand, we also collected far-UV CD spectra of the wild-type MSP domain in the presence of DPC at different ratios (Fig. 1C). However, with the ratio up to 1:200 (MSP:DPC), its native structure still remains almost unchanged (Fig. 1C). Further addition of DPC resulted in visible aggregation even at a protein concentration of only 20 μM for CD experiments.

3.2. Conformational transformations as monitored by NMR spectroscopy

We subsequently characterized the transformation by acquiring $^{1}H–^{15}N$ two-dimensional HSQC spectra at a protein concentration of 100 μM in the absence and in the presence of DPC at different ratios. For the wild-type MSP domain, no HSQC peak shifts occurred with ratios up to 1:50. On the other hand, further increasing the ratios resulted in visible aggregates in the NMR tube. Nevertheless, even with visible aggregates, only the intensity of HSQC peaks uniformly decreased but their positions remain almost unshifted (spectra not shown). This indicates that the well-folded MSP domain had no specific interaction with DPC molecules but however high DPC concentrations would lead to a very hydrophobic environment which unavoidably triggered non-specific aggregation as the solvent exposed side chains are mostly hydrophilic in a well-folded protein such as the wild-type MSP domain.

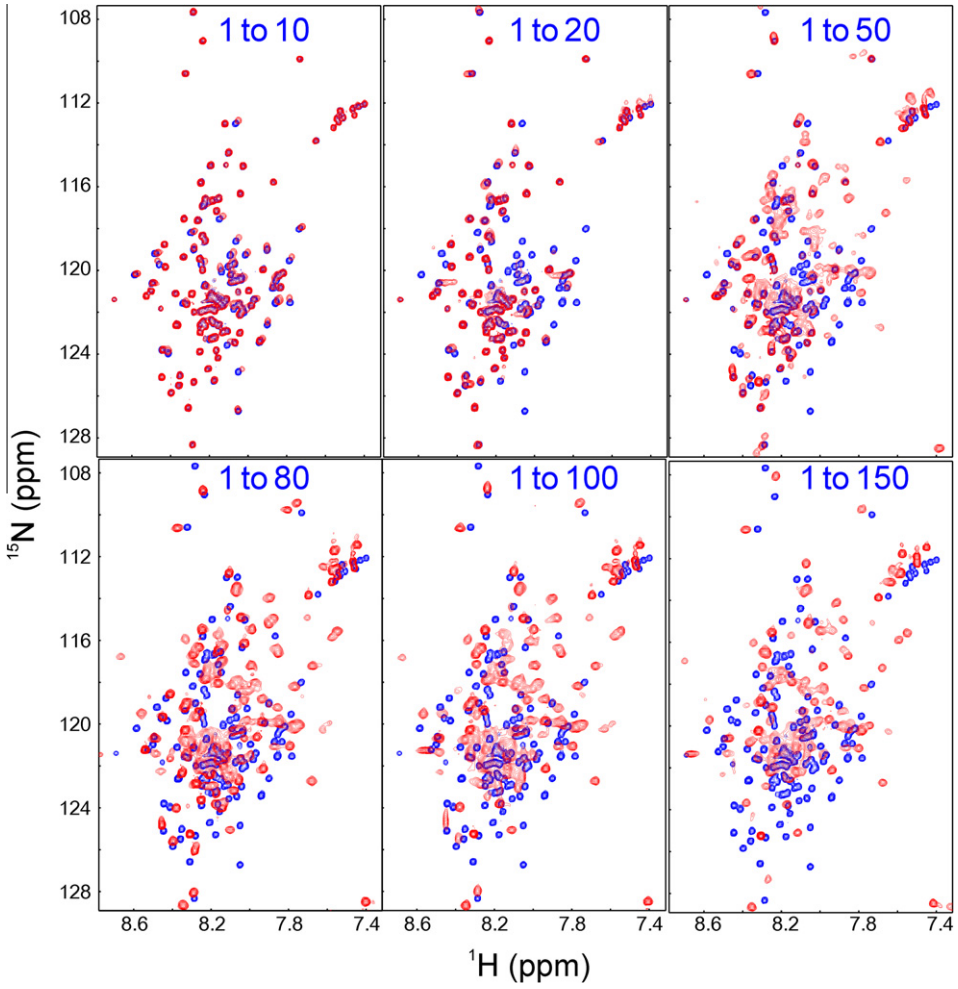

Fig. 2. $^{1}H–^{15}N$ NMR HSQC spectra of P56S-MSP in the absence of (blue) and presence of DPC at different ratios (red) as indicated (P56S:DPC). (For interpretation of the references to colour in this figure legend, the reader is referred to the web version of this article.)

By contrast, as seen in Fig. 2, several HSQC peaks shifted at a ratio of 1:10 (P56S:DPC), implying that these residues started to interact with DPC molecules. At 1:20, many HSQC peaks disappeared, suggesting that these residues interact with DPC molecules or/and undergo conformational exchanges over μs-ms time scale which make their HSQC peaks too broad to be detected. Interestingly, at a ratio of 1:50 many peaks reappeared but almost all HSQC peaks shifted to some degree. This suggests that at high ratios, most P56S-MSP residues are involved in interacting with DPC, or/and conformational changes. Furthermore, the HSQC spectra at 1:80 and 1:150 are highly similar, implying that the conformational transformation is indeed largely completed at 1:80, consistent with the CD results.

The similar changes were observed for the HSQC spectra of VAPB-3 upon gradual addition of DPC (Fig. 3). However, it appears that the HSQC peaks of VAPB-3 are more broadening than those of P56S-MSP, indicating that there exist more profound conformational exchanges on μs-ms for VAPB-3 in the presence of DPC. We also collected HSQC spectra of P56S-MSP and VAPB-3 at a protein concentration of 1 mM and DPC concentration of 150 mM, but their HSQC spectra are almost superimposible to the corresponding ones at a protein concentration of 100 μM and DPC concentration of 15 mM. This strongly implies that no severe aggregation is associated with the helical conformations formed in membrane environment. Interestingly for both P56S-MSP and VAPB-3, only one set of HSQC peaks were observed upon adding DPC, suggesting that the conformational transformation is a gradual process or/and within fast exchange regime on NMR time scale.

3.3. Residue-specific conformation of VAPB-3 in water

Although VAPB-3 has a narrowly-dispersed HSQC spectrum in water (Fig. 4A), we have successfully achieved the sequential assignment of most residues with a pair of triple resonance experiments HNCACB and CBCA(CO)NH. Subsequently we assigned all NOE connectivities by analyzing HSQC–TOCSY and HSQC–NOESY spectra. It is well-established that the difference between $C\alpha$ and $C\beta$ chemical shift deviations from their corresponding random-coil values is very sensitive indicators of protein secondary structures [25–27], thus representing a powerful probe for detecting residual secondary structures in unfolded or partially folded proteins.

As seen in Fig. 4B, very small ($\Delta C\alpha - \Delta C\beta$) values over the majority of VAPB-3 residues clearly indicate that it is highly unstructured in water, completely consistent with CD results. Interestingly, if excluding the previously-unassigned regions in P56S-MSP, the N-terminal 105 residues of VAPB-3 have a ($\Delta C\alpha - \Delta C\beta$) pattern similar to that of P56S-MSP except for some large variations close to the residue 56 which is Pro in VAPB-3 and Ser in P56S-MSP. Furthermore, the lacking of stable secondary structures in VAPB-3 is strongly demonstrated by the NOE patterns defining the secondary structures (Fig. 4C). For most residues, only sequential NOEs could be identified. Only over several short segments, NOE $d_{\alpha N}(i, i+2)$ but not NOE $d_{\alpha N}(i, i+3)$ were found, indicating that dynamic helical conformation is weakly populated over these regions [18,22–24]. No long-range NOE was detected, as expected for such a predominantly-disordered protein without any tight tertiary structure.

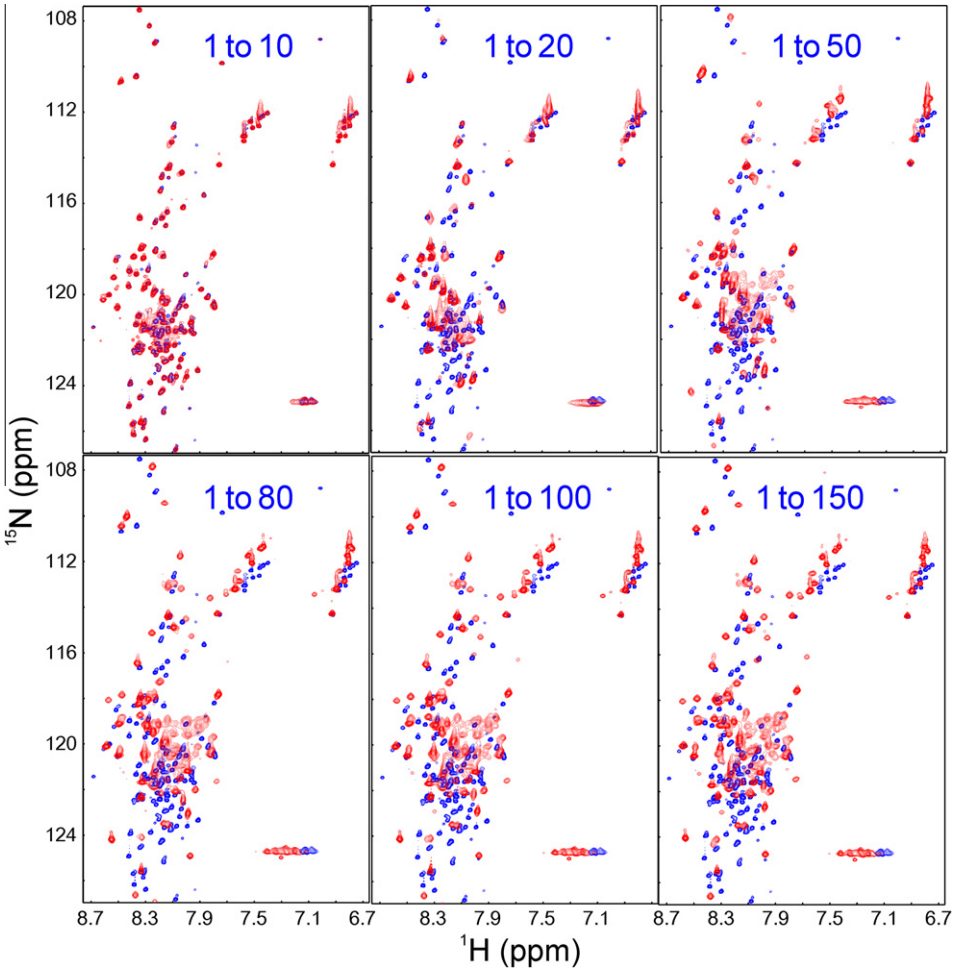

Fig. 3. ^{1}H–^{15}N NMR HSQC spectra of VAPB-3 in the absence of (blue) and presence of DPC at different ratios (red) as indicated (VAPB-3:DPC). (For interpretation of the references to colour in this figure legend, the reader is referred to the web version of this article.)

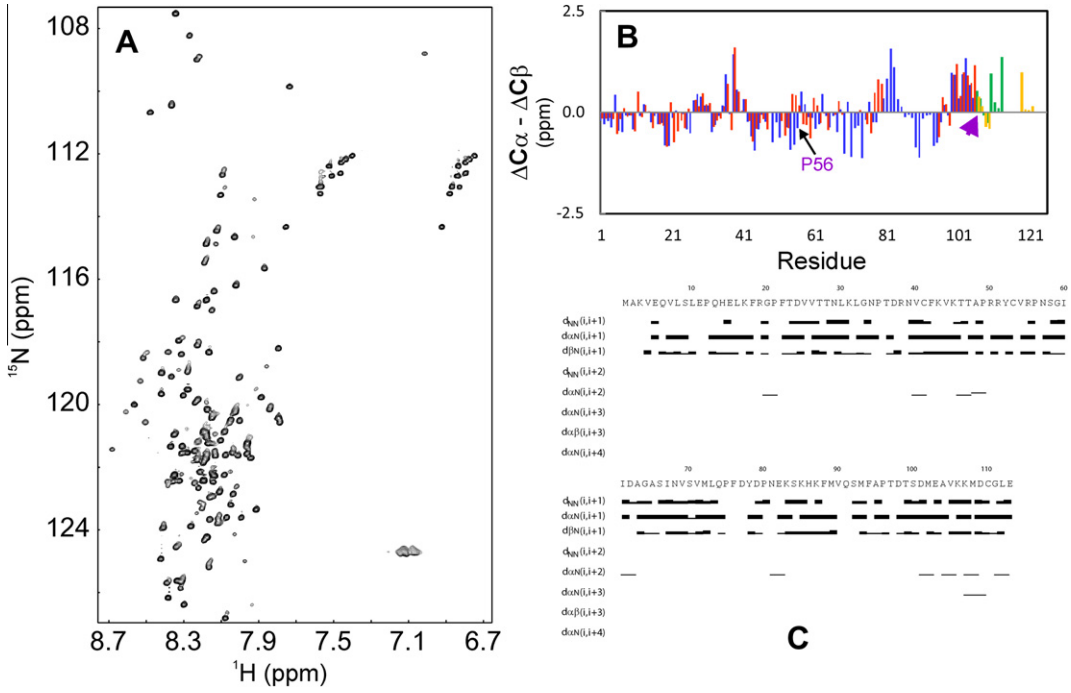

Fig. 4. Residue-specific conformation of VAPB-3 in water. (A) ^{1}H–^{15}N NMR HSQC spectrum of VAPB-3 acquired at 25 °C. (B) Residue specific (ΔCα–ΔCβ) values. For VAPB-3, green bars are used to indicate (ΔCα–ΔCβ) values for the first 105 residues identical to those of MSP, while green bars for unique residues. For P56S-MSP, red bars are used to indicate (ΔCα–ΔCβ) values for the first 105 residues, while brown bars for the C-terminal 20 residues. (C) NOE connectivity pattern of VAPB-3 defining secondary structures. (For interpretation of the references to colour in this figure legend, the reader is referred to the web version of this article.)

4. Discussion

Despite intense studies after ALS was first described more than 130 years ago, its underlying mechanism still remains a mystery. Successful identification of genetic mutations on a variety of proteins from familial ALS patients remarkably facilitate of our understanding of the ALS pathogenesis. The effects of the inherited disease-causative mutants can be explained by loss of function or/and gain of function or/and by a combination of both [20]. As for ALS8, we previously demonstrated that the P56S mutation eliminated its native β-structure and led to a complete loss of the binding ability to FFAT-motif containing peptide and EphA4 receptors *in vitro* [18]. Although like all other neurodegenerative diseases, ALS is also characteristic of severe aggregation of mutated proteins such as SOD1 and VAPB mutants, the mechanisms by which the aggregated proteins gain new functions are poorly defined. For ALS8, the accumulation of aggregated inclusions has been extensively demonstrated in cells and thus been proposed to trigger ALS pathogenesis through unfolded protein response (UPR) in ER [16,17]. Amazingly, however, a recent study detected no accumulation of cytoplasmic aggregates of the P56S mutant in induced stem cells of ALS8 patients [19]. Therefore, currently no mechanism exists to rationalize a recent observation that the P56S mutant is able to uniquely restructure ER cisternae although the aggregates get cleaved rapidly in the cells [20].

Here our study presents the first evidence that the P56S-MSP and VAPB-3, but not the wild-type MSP, can interact with lipid molecules and subsequently transform into highly-helical conformations in a membrane environment without any detectable aggregation. This provides a molecular mechanism to rationalize the surprising observation that the P56S mutant has a unique ability to specifically remodel ER structure. It is likely that the ability of P56S mutant to change ER structure is resulting from its specific interaction with ER membrane. On the other hand, the result that VAPB-3 shares the similar properties of P56S-MSP such as to interact with membrane implies a potential mechanism underlying sporadic ALS. Previously, it was shown that the VAPB-3 protein becomes detectable in cells upon proteasomal inhibition, a condition commonly found in neurodegenerative diseases [6]. This means that even without carrying any ALS-causative mutation, a person might develop ALS through a mechanism underlying ALS8, if VAPB slicing variants like VAPB-3 get accumulated in cells to a certain degree, due to proteasomal inhibition triggered by pathological or/and environmental conditions.

The present discovery is also of fundamental interest for understanding protein folding. As previously demonstrated [18], the wild-type MSP domain adopts a well-defined fold constituted by only β-strands. Surprisingly as we deciphered here, a single-residue P56S mutation is sufficient to transform it into a membrane-interacting protein with a highly helical conformation. Moreover, the truncation of the MSP domain in VAPB-3 also results in the similar transformation. This implies that the MSP sequence has the chameleon capacity to adopt two structures: a β-sandwich fold and a membrane-stabilized helical structure upon the MSP tertiary structure being disrupted by the P56S mutation or truncation.

Involvement of membranes has been increasingly recognized in other diseases including neurodegenerative diseases, as evidenced from extensive biophysical investigations on the interactions of amyloid peptides and prion protein with membranes [28,29]. Despite the challenge to determine the structure of a protein of >100 residues in a membrane environment, currently we are focused on optimizing experimental conditions in order to obtain high-quality NMR spectra which allow sequential assignment and subsequent calculation of the structures of P56S-MSP or/and VAPB-3 in DPC.

Acknowledgments

This study is supported by Ministry of Education of Singapore Tier 2 Grant MOE2011-T2-1-096 to J. Song.

References

[1] L.I. Bruijn, T.M. Miller, D.W. Cleveland, Unraveling the mechanisms involved in motor neuron degeneration in ALS, Annu. Rev. Neurosci. 27 (2004) 723–749.

[2] P. Pasinelli, R.H. Brown, Molecular biology of amyotrophic lateral sclerosis: insights from genetics, Nat. Rev. Neurosci. 7 (2006) 710–723.

[3] P.M. Andersen, A. Al-Chalabi, Clinical genetics of amyotrophic lateral sclerosis: what do we really know?, Nat Rev. Neurol. 7 (2011) 603–615.

[4] A.L. Nishimura, M. Mitne-Neto, H.C. Silva, et al., A mutation in the vesicle trafficking protein VAPB causes late onset spinal muscular atrophy and amyotrophic lateral sclerosis, Am. J. Hum. Genet. 75 (2004) 822–831.

[5] Y. Nishimura, M. Hayashi, H. Inada, et al., Molecular cloning and characterization of mammalian homologues of vesicle-associated membrane protein-associated (VAMP-associated) proteins, Biochem. Biophys. Res. Commun. 254 (1999) 21–26.

[6] T. Nachreiner, M. Esser, V. Tenten, et al., Novel splice variants of the amyotrophic lateral sclerosis-associated gene VAPB expressed in human tissues, Biochem. Biophys. Res. Commun. 394 (2010) 703–708.

[7] P.A. Skehel, R. Fabian-Fine, E.R. Kandel, Mouse VAP33 is associated with the endoplasmic reticulum and microtubules, Proc. Natl. Acad. Sci. USA 97 (2000) 1101–1106.

[8] C.J. Loewen, T.P. Levine, A highly conserved binding site in vesicle-associated membrane protein-associated protein (VAP) for the FFAT motif of lipid-binding proteins, J. Biol. Chem. 280 (2005) 14097–14104.

[9] H. Tsuda, S.M. Han, Y. Yang, et al., The amyotrophic lateral sclerosis 8 protein VAPB is cleaved, secreted, and acts as a ligand for Eph receptors, Cell 133 (2008) 963–977.

[10] S. Lua, H. Qin, L. Lim, et al., Structural, stability, dynamic and binding properties of the ALS-causing T46I mutant of the hVAPB MSP domain as revealed by NMR and MD simulations, PLoS One 6 (2011) e27072.

[11] E.B. Pasquale, Eph–Ephrin bidirectional signaling in physiology and disease, Cell 133 (2008) 38–52.

[12] H. Qin, J. Shi, R. Noberini, et al., Crystal structure and NMR binding reveal that two small molecule antagonists target the high affinity Ephrin-binding channel of the EphA4 receptor, J. Biol. Chem. 283 (2008) 29473–29484.

[13] S.M. Han, H. Tsuda, Y. Yang, et al., Secreted VAPB/ALS8 major sperm protein domains modulate mitochondrial localization and morphology via growth cone guidance receptors, Dev. Cell 22 (2012) 348–362.

[14] G. Gupta, H. Qin, J. Song, Intrinsically unstructured domain 3 of hepatitis C virus NS5A forms a "fuzzy complex" with VAPB-MSP domain which carries ALS-causing mutations, PLoS One 7 (2012) e39261.

[15] H.J. Chen, G. Anagnostou, A. Chai, et al., Characterization of the properties of a novel mutation in VAPB in familial amyotrophic lateral sclerosis, J. Biol. Chem. 285 (2010) 40266–40281.

[16] E. Teuling, S. Ahmed, E. Haasdijk, et al., Motor neuron disease-associated mutant vesicle-associated membrane protein- associated protein (VAP) B recruits wild-type VAPs into endoplasmic reticulum-derived tubular aggregates, J. Neurosci. 27 (2007) 9801–9815.

[17] K. Kanekura, H. Suzuki, S. Aiso, et al., ER stress and unfolded protein response in amyotrophic lateral sclerosis, Mol. Neurobiol. 39 (2009) 81–89.

[18] J. Shi, S. Lua, J.S. Tong, et al., Elimination of the native structure and solubility of the hVAPB MSP domain by the Pro56Ser mutation that causes amyotrophic lateral sclerosis, Biochemistry 49 (2010) 3887–3897.

[19] M. Mitne-Neto, M. Machado-Costa, M.C.N. Marchetto, et al., Downregulation of VAPB expression in motor neurons derived from induced pluripotent stem cells of ALS8 patients, Hum. Mol. Genet. 20 (2011) 3642–3652.

[20] G. Papiani, A. Ruggiano, M. Fossati, et al., Restructured endoplasmic reticulum generated by mutant amyotrophic lateral sclerosis-linked VAPB is cleared by the proteasome, J. Cell Sci. 125 (2012) 3601–3611.

[21] C.N. Pace, F. Vajdos, L. Fee, et al., How to measure and predict the molar absorption coefficient of a protein, Protein Sci. 4 (1995) 2411–2423.

[22] N. Sreerama, R.W. Woody, Estimation of protein secondary structure from CD spectra: comparison of CONTIN, SELCON and CDSSTR methods with an expanded reference set, Anal. Biochem. 282 (2000) 252–260.

[23] J. Song, Insight into "insoluble proteins" with pure water, FEBS Lett. 583 (2009) 953–959.

[24] K. Delak, C. Harcup, R. Lakshminarayanan, et al., The tooth enamel protein, porcine amelogenin, is an intrinsically disordered protein with an extended molecular configuration in the monomeric form, Biochemistry 48 (2009) 2272–2281.

[25] H.J. Dyson, P.E. Wright, Unfolded proteins and protein folding studied by NMR, Chem. Rev. 104 (2004) 3607–3622.

[26] Y. Bai, J. Chung, H.J. Dyson, P.E. Wright, Structural and dynamic characterization of an unfolded state of poplar apo plastocyanin formed under nondenaturing conditions, Protein Sci. 10 (2001) 1056–1066.

[27] J. Liu, J. Song, NMR evidence for forming highly populated helical conformations in the partially folded hNck2 SH3 domain, Biophys. J. 95 (2008) 4803–4812.

[28] R.P. Nanga, J.R. Brender, J. Xu, et al., Three-dimensional structure and orientation of rat islet amyloid polypeptide protein in a membrane environment by solution NMR spectroscopy, J. Am. Chem. Soc. 131 (2009) 8252–8261.

[29] K. Elfrink, J. Ollesch, J. Stöhr, et al., Structural changes of membrane-anchored native PrP(C), Proc. Natl. Acad. Sci. USA 105 (2008) 10815–10819.